mathematics

MDPI

Article

Outage Analysis of LEO Satellite Association Schemes Using Stochastic Geometry

Jonghyun Bang [1] **and Taehyoung Kim** [2,*]

[1] Department of Electronic Engineering, Myongji University, Yongin 17058, Republic of Korea; jhyun@mju.ac.kr
[2] School of Electrical Engineering, Kookmin University, Seoul 02707, Republic of Korea
* Correspondence: th.kim@kookmin.ac.kr

Abstract

This paper investigates the outage performance of large-scale low-Earth-orbit (LEO) satellite constellations using a stochastic-geometry framework. The ground-projected satellite distribution is modeled as a Poisson point process (PPP) that captures finite visibility and beam-hopping activity. Analytical outage expressions and approximations are developed under shadowed-Rician (SR) fading for two representative user–satellite association schemes: the optimal best-association rule and the practical nearest-association rule. For the latter, an Equivalent Integration Point (EIP) approximation is developed, replacing the outer serving-distance integral with a single evaluation at a representative distance, providing accurate yet tractable performance evaluation. Monte Carlo simulation results confirm the accuracy of the EIP approximation and demonstrate that nearest association offers a practical trade-off between reliability and selection complexity by requiring only distance information rather than instantaneous signal-to-interference ratio (SIR) evaluation.

Keywords: LEO satellite networks; non-terrestrial networks (NTNs); stochastic geometry; outage probability; beam hopping; user association

MSC: 94A05

1. Introduction

The advent of low-Earth-orbit (LEO) satellite constellations has ushered in a new era of global communications, enabling low-latency, high-throughput connectivity across terrestrial and remote regions [1,2]. Motivated by these advances, recent studies have explored diverse LEO networking paradigms, including broadband access through large-scale constellations [3], random access for non-terrestrial uplinks [4], and system-level design for integrated terrestrial–satellite networks [5].

As the number of deployed LEO satellites increases, user–satellite association becomes a critical design challenge, since multiple satellites can be simultaneously visible and resources are reused under beam hopping and spectrum sharing [6]. Recent studies have investigated complementary aspects of this problem, including coordinated beam scheduling [7], cooperative beam association and power allocation in ultra-dense LEO networks [8], beam-hopping resource allocation under co-channel interference [9], and real-time user–satellite assignment for handover management [10]. Stochastic-geometry-based approaches have also been employed to analyze LEO routing and access performance [11,12], while broader studies have examined the deployment and propagation challenges of non-terrestrial network (NTN) systems [13].

Check for updates

Academic Editors: Alexander Zeifman and Mark Kelbert

Received: 4 September 2026
Revised: 12 October 2026
Accepted: 22 October 2026
Published: 26 October 2026

Copyright: © 2026 by the authors. Licensee MDPI, Basel, Switzerland. This article is an open access article distributed under the terms and conditions of the Creative Commons Attribution (CC BY) license.

More directly related to the present work, Okati et al. [14] analyze downlink coverage and rate under nearest-satellite association using a spherical binomial point process model. Kim et al. [15] characterize desired and interfering signal powers under shadowed-Rician (SR) fading for multiple spot beams transmitted by a single LEO satellite. However, these studies do not directly compare best association based on the instantaneous signal-to-interference ratio (SIR) with distance-based nearest association under the joint effects of finite visibility, random beam activity, and both co-channel and leakage interference. Consequently, analytically characterizing the reliability–complexity trade-off between these association strategies in dense LEO constellations remains an important problem.

This gap motivates our work, which aims to establish an analytically tractable model for evaluating user–satellite association strategies in large-scale LEO constellations. Specifically, we examine average outage over spatial configurations and beam-activity realizations and its dependence on network parameters. While deterministic constellation models are suited to evaluating a specified orbital deployment and user location, stochastic geometry facilitates this analysis through a tractable characterization of serving-candidate availability and aggregate interference.

To this end, we develop a stochastic-geometry-based analytical framework that models the ground-projected satellite distribution as a homogeneous Poisson point process (PPP) and investigates two representative association strategies: (i) an *optimal best-association* rule that maximizes the SIR, and (ii) a *practical nearest-association* rule that selects the serving satellite solely based on projected distance. While best association requires instantaneous channel-quality information from all visible satellites, nearest association relies only on geometric proximity, reducing both signaling overhead and analytical complexity in rapidly varying LEO environments.

The main contributions are summarized as follows:

- **System modeling:** A tractable stochastic-geometry-based model for LEO downlink communications is established, capturing the effects of finite visibility, beam-hopping activity, and both co-channel and leakage interference under normalized SR fading.
- **Analytical framework:** A tractable outage probability approximation is derived for the best-association rule, and an integral outage expression is obtained for the nearest-association rule. An Equivalent Integration Point (EIP) approximation is developed to replace the outer serving-distance average with a single evaluation at a representative distance. This distance is defined as the root-mean-square projected serving distance, conditioned on the existence of a visible co-channel satellite. The interference integrals and finite SR sums are retained.
- **Design insights:** Nearest association offers a practical reliability–complexity trade-off, requiring only distance information at the cost of higher outage than best association. For nearest association, increasing satellite density initially improves reliability, but excessive densification eventually increases outage as aggregate interference grows. The reuse-factor results further reveal a balance between co-channel interference reduction and serving-candidate availability.

The remainder of this paper is organized as follows. Section 2 presents the system model, including the satellite visibility, beam-hopping, frequency-reuse, and interference models. Section 3 derives the outage performance of the best- and nearest-association schemes and develops the EIP approximation for nearest association. Section 4 presents the numerical and simulation results and discusses the impact of key system parameters. Finally, Section 5 concludes the paper.

2. System Model

We consider a downlink LEO NTN in which a large number of satellites are deployed in orbit at altitude H, each transmitting with equal power P_t as shown in Figure 1. From the perspective of a ground user, the relevant geometry is given by the projection of satellites onto the Earth's surface. For analytical tractability, we model the *ground-projected satellite positions* as a homogeneous PPP $\Phi \subset \mathbb{R}^2$ with intensity λ_{sat} [sat/km^2]. Such stochastic-geometry-based abstractions provide a tractable means of characterizing large-scale LEO network performance [11,14,16,17]. In addition, a typical user is assumed to be located at the origin on the ground plane.

Let ρ denote the ground-projected distance between the typical user and a projected satellite. Then, the corresponding user–satellite distance is defined by

$$r(\rho) = \sqrt{H^2 + \rho^2}. \tag{1}$$

Furthermore, the elevation angle observed by the user is

$$\theta(\rho) = \arctan\left(\frac{H}{\rho}\right). \tag{2}$$

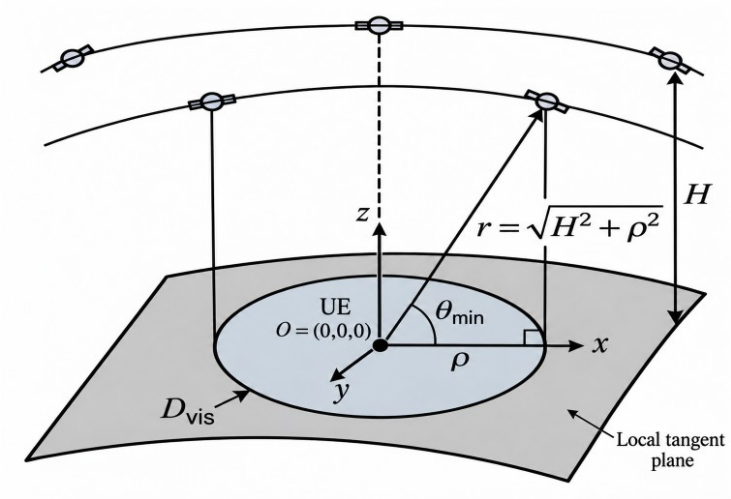


Figure 1. 3D visibility geometry and ground-projected model for the LEO satellite network. The typical user equipment (UE) is located at the origin of a local tangent plane. The visibility disk $\mathcal{D}_{\text{vis}}$ is defined by the satellite altitude H and the minimum elevation angle $\theta_{\min}$. The slant distance r is uniquely determined by the projected ground distance ρ via $r = \sqrt{H^2 + \rho^2}$. The vertical dashed line represents the normal projection from the zenith satellite to the user plane.

We define the minimum elevation angle $\theta_{\min}$ as the smallest elevation above the horizon at which the terminal can maintain a communication link. A minimum elevation $\theta_{\min}$ ensures robustness against terrain blockage and horizon losses [18]. This constraint determines which satellites are visible from the user's perspective. Geometrically, it defines a visibility region on the ground plane. Under the adopted local planar-Earth approximation, the associated visibility radius is given by

$$R_{\text{vis}} = \frac{H}{\tan\theta_{\min}}. \tag{3}$$

Accordingly, the visibility region is defined as

$$\mathcal{D}_{\text{vis}} = \left\{ x \in \mathbb{R}^2 : \|x\| \le R_{\text{vis}} \right\}. \tag{4}$$

Note that only satellites located within $\mathcal{D}_{\text{vis}}$ are eligible for service.

In practice, satellites cannot activate all beams simultaneously and may employ *beam hopping* (time-slot beam scheduling) [18,19]. We model this operation by assuming that, in each time slot, a visible satellite has an active beam on the considered resource with probability $p \in (0, 1]$, independently across satellites. Under this independent-thinning approximation, the active satellite process is a PPP with intensity

$$\lambda_{\text{act}} = \lambda_{\text{sat}} p. \tag{5}$$

With a frequency-reuse factor $F \geq 1$, we assume that each active satellite is independently assigned to one of the F frequency groups with equal probability. By the independent marking property of a PPP, the active process is partitioned into two independent PPPs:

- *Co-channel set*: satellites using the same carrier as the user, with intensity $\lambda_c = \lambda_{\text{act}}/F$.
- *Leakage-interference set*: satellites using other carriers, contributing leakage interference with intensity $\lambda_\ell = \lambda_{\text{act}}(1 - 1/F)$.

We adopt SR fading with common parameters (b, Ω, m) to account for a fluctuating line-of-sight component and diffuse scattering [15,20]. The channel power gains h_s are normalized such that $\mathbb{E}[h_s] = 1$ and are independent across satellites and independent of their locations and activity marks. Here, $2b$ and Ω denote the average diffuse and line-of-sight powers before normalization, respectively, while m is the shadowing shape parameter.

The received power from a satellite at distance r is expressed as

$$P_{\text{rx}} = P_t \, G \, h \, r^{-\alpha}, \tag{6}$$

where α denotes the path-loss exponent and G represents the effective antenna gain. Following [18], the gains for the serving, co-channel, and leakage links are denoted by G_0, G_I, and βG_I $(0 < \beta < 1)$, respectively. The serving beam is assumed to be perfectly steered toward the user, and a unit isotropic receive gain is assumed. Thus, G_0 represents the boresight transmit gain.

We write $r(x) \triangleq r(\|x\|)$ for the slant distance of a satellite at projected location x. The instantaneous SIR of a candidate satellite $s \in \Phi_c$ with fading gain h_s is

$$\text{SIR}(s) = \frac{P_t G_0 h_s r(s)^{-\alpha}}{I_c + I_\ell}, \tag{7}$$

where

$$\begin{aligned} I_c &= \sum_{u \in \Phi_c \setminus \{s\}} P_t G_I h_u r(u)^{-\alpha}, \\ I_\ell &= \sum_{v \in \Phi_\ell} P_t (\beta G_I) h_v r(v)^{-\alpha}, \end{aligned} \tag{8}$$

and Φ_c and Φ_ℓ denote the co-channel and leakage interferer PPPs within $\mathcal{D}_{\text{vis}}$.

We focus on the interference-limited regime typical of dense beam-hopping LEO systems, where aggregate inter-beam interference dominates over thermal noise; the main analysis therefore focuses on SIR. A brief extension to the signal-to-interference-plus-noise ratio (SINR) is presented after Lemma 4. For convenience, the main notation used throughout the paper is summarized in Appendix A.

3. Outage Performance Analysis of LEO Association Schemes

In this section, we analyze the outage probability under two representative satellite-association strategies: (i) the *best association* and (ii) the *nearest association*.

3.1. Best Association

We first consider the *best-association* rule, in which the user connects to the active co-channel satellite that maximizes the instantaneous SIR:

$$s^\star = \arg\max_{s\in\Phi_c} \mathrm{SIR}(s), \qquad \rho^\star = \|s^\star\|. \tag{9}$$

For the best-association rule, the user connects to the visible satellite that yields the highest instantaneous SIR. Hence, an outage occurs when even the strongest SIR among all visible co-channel satellites fails to exceed the decoding threshold τ; in other words, no satellite can provide a sufficient link quality for successful decoding and its outage probability can be represented as

$$P_{\mathrm{out}}^{\mathrm{best}}(\tau) = \mathbb{P}\Big[\max_{s\in\Phi_c} \mathrm{SIR}(s) < \tau\Big]. \tag{10}$$

Because the SIR events of different candidate satellites are correlated, an exact evaluation of (10) is generally intractable. We therefore adopt an independence approximation across candidate-link success events to obtain a tractable analytical expression.

Lemma 1. *For a candidate active co-channel satellite at projected distance $0 \le \rho \le R_{\mathrm{vis}}$, under normalized SR fading with $m \in \mathbb{N}_+$, the conditional success probability is*

$$p_{\mathrm{succ}}^{\mathrm{best}}(\rho;\tau) = \sum_{n=0}^{m-1} c_n \frac{(-z)^n}{n!} \frac{d^n}{dz^n}\Big[\mathcal{L}_{I_c}^{\mathrm{best}}(z)\mathcal{L}_{I_\ell}(z)\Big]\Big|_{z=z_\rho}, \tag{11}$$

where

$$\mathcal{L}_{I_c}^{\mathrm{best}}(z) = \exp\Big[-2\pi\lambda_c \int_0^{R_{\mathrm{vis}}} \big\{1 - \mathcal{L}_h(zC_c r(t)^{-\alpha})\big\}\, t\, dt\Big], \tag{12}$$

$$\mathcal{L}_{I_\ell}(z) = \exp\Big[-2\pi\lambda_\ell \int_0^{R_{\mathrm{vis}}} \big\{1 - \mathcal{L}_h(zC_\ell r(t)^{-\alpha})\big\}\, t\, dt\Big]. \tag{13}$$

Here, $C_c = P_t G_I$, $C_\ell = P_t \beta G_I$, and

$$z_\rho = \frac{\tau r(\rho)^\alpha}{P_t G_0 \vartheta}, \qquad \vartheta = \frac{2b + \Omega/m}{2b + \Omega}. \tag{14}$$

The coefficients c_n and the channel Laplace transform $\mathcal{L}_h$ are specified in (16) and (17), respectively.

Proof. Integrating the integer-order SR power density in [15] after unit-mean normalization gives

$$\overline{F}_h(x) = e^{-x/\vartheta} \sum_{n=0}^{m-1} c_n \frac{(x/\vartheta)^n}{n!}, \qquad x \ge 0, \tag{15}$$

where

$$c_n = \sum_{j=n}^{m-1} \binom{m-1}{j} \xi^j (1-\xi)^{m-1-j}, \qquad n = 0, \ldots, m-1, \tag{16}$$

and $\xi = \Omega/(2bm + \Omega)$. The normalized SR power gain has the Laplace transform [20]

$$\mathcal{L}_h(u) = \frac{\left(1 + \dfrac{2bu}{2b+\Omega}\right)^{m-1}}{(1+\vartheta u)^m}, \qquad u \ge 0. \tag{17}$$

By Slivnyak's theorem [16,17], conditioning on the candidate imposes no exclusion region on the remaining co-channel PPP. Applying the PPP probability generating functional (PGFL) with (17) to each interferer process gives (12) and (13) over the full visibility disk [16,17].

Let $I = I_c + I_\ell$. Since h_s is independent of I, using (7) and (15) yields

$$\begin{aligned} p_{\mathrm{succ}}^{\mathrm{best}}(\rho;\tau) &= \mathbb{E}_I\big[\overline{F}_h(\vartheta z_\rho I)\big] \\ &= \sum_{n=0}^{m-1} c_n \frac{z_\rho^n}{n!} \mathbb{E}_I\Big[I^n e^{-z_\rho I}\Big]. \end{aligned} \tag{18}$$

Finally, independence of the two interferer processes and differentiation of their Laplace transforms give

$$\mathbb{E}_I\Big[I^n e^{-zI}\Big] = (-1)^n \frac{d^n}{dz^n}\Big[\mathcal{L}_{I_c}^{\mathrm{best}}(z)\mathcal{L}_{I_\ell}(z)\Big]. \tag{19}$$

Substituting this identity into (18) yields (11). □

Lemma 2. *Under the independence approximation, the outage probability for the best-association rule is*

$$\widetilde{P}_{\mathrm{out}}^{\mathrm{best}}(\tau) = \exp\left[-\int_0^{R_{\mathrm{vis}}} 2\pi\lambda_c\rho\, p_{\mathrm{succ}}^{\mathrm{best}}(\rho;\tau)\, d\rho\right]. \tag{20}$$

Proof. Under the independence approximation, each co-channel satellite at projected distance ρ is treated as independently successful with probability $p_{\mathrm{succ}}^{\mathrm{best}}(\rho;\tau)$. Accordingly, the original PPP Φ_c of intensity λ_c is approximated by an inhomogeneously thinned PPP with local intensity $\lambda_c p_{\mathrm{succ}}^{\mathrm{best}}(\rho;\tau)$ within $\mathcal{D}_{\mathrm{vis}}$.

The outage event $\{\max_{s\in\Phi_c} \mathrm{SIR}(s) < \tau\}$ corresponds to having no successful candidate satellite in $\mathcal{D}_{\mathrm{vis}}$. Therefore,

$$\mathbb{P}\big[N_{\mathrm{succ}}(\mathcal{D}_{\mathrm{vis}}) = 0\big] = \exp\left(-\int_{\mathcal{D}_{\mathrm{vis}}} \lambda_c p_{\mathrm{succ}}^{\mathrm{best}}(\|x\|;\tau)\, dx\right).$$

Converting the spatial integral into polar coordinates yields (20). □

Remark 1. *From (20), the outage probability decreases with the active satellite density $\lambda_{\mathrm{sat}}p$ in the low-density regime, since denser constellations increase the chance of finding a strong serving link. As the density increases, however, aggregate interference also grows and can offset the benefit of having more serving candidates. The benefit of densification therefore depends on the balance between improved serving-link selection and increased interference.*

3.2. Nearest Association

While the best-association rule yields the highest performance by comparing the instantaneous SIRs of all visible satellites, acquiring such full SIR information is impractical in fast-moving LEO systems due to rapid channel variations and signaling overhead. To enable low-complexity association, we instead consider a distance-based rule that relies only on satellite positions. Specifically, when $\Phi_c \neq \varnothing$, the user associates with the nearest co-channel active satellite:

$$s_0 = \arg\min_{s\in\Phi_c} \|s\|, \qquad \rho_0 = \|s_0\|, \qquad 0 \le \rho_0 \le R_{\mathrm{vis}}.$$

If $\Phi_c = \varnothing$, we set $\rho_0 = \infty$ and count the event as an outage. In the nearest-association rule, the user connects to the closest co-channel active satellite rather than comparing all SIR values. The outage event therefore occurs when this nearest satellite fails to provide an SIR above the decoding threshold τ.

For the nearest-association rule, conditioning on $\rho_0 = \rho$ implies that no other co-channel satellite exists within the disk of radius ρ. Using the same argument as in Lemma 1, the conditional success probability for $m \in \mathbb{N}_+$ can then be expressed as

$$p_{\text{succ}}^{\text{nearest}}(\rho;\tau) = \sum_{n=0}^{m-1} c_n \frac{(-z)^n}{n!} \frac{\partial^n}{\partial z^n} \left[\mathcal{L}_{I_c}^{\text{nearest}}(z \mid \rho)\mathcal{L}_{I_\ell}(z)\right]\Big|_{z=z_\rho}, \tag{21}$$

where

$$\mathcal{L}_{I_c}^{\text{nearest}}(z \mid \rho) = \exp\left[-2\pi\lambda_c \int_\rho^{R_{\text{vis}}} \left\{1 - \mathcal{L}_h(zC_c r(t)^{-\alpha})\right\} t\, dt\right]. \tag{22}$$

The leakage transform $\mathcal{L}_{I_\ell}(z)$ remains as given in (13), since conditioning on ρ_0 does not affect the independent leakage-interference process. Here, z_ρ, c_n, and $\mathcal{L}_h$ are defined in (14), (16), and (17), respectively. The derivatives are taken with respect to z while holding ρ fixed.

Lemma 3. *The outage probability of the nearest-association rule can be defined as*

$$P_{\text{out}}^{\text{nearest}}(\tau) = 1 - \int_0^{R_{\text{vis}}} 2\pi\lambda_c \rho e^{-\pi\lambda_c\rho^2} p_{\text{succ}}^{\text{nearest}}(\rho;\tau)\, d\rho. \tag{23}$$

Proof. The outage probability under the nearest-association rule is defined as

$$P_{\text{out}}^{\text{nearest}}(\tau) = 1 - \mathbb{P}[\rho_0 \le R_{\text{vis}}, \text{SIR}(s_0) \ge \tau], \tag{24}$$

where ρ_0 denotes the distance to the nearest visible co-channel satellite.

In a PPP of intensity λ_c confined to the visibility disk $\mathcal{D}_{\text{vis}}$, the probability that at least one co-channel satellite exists is

$$\mathbb{P}\left[\rho_0 \le R_{\text{vis}}\right] = 1 - e^{-A}. \tag{25}$$

Here, $A \triangleq \pi\lambda_c R_{\text{vis}}^2$ is a constant, and this result follows directly from the void probability of a PPP. Conditioned on this event, the nearest-distance probability density function (PDF) becomes

$$f_{\rho_0|\text{vis}}(\rho) = \frac{2\pi\lambda_c\rho\, e^{-\pi\lambda_c\rho^2}}{1 - e^{-A}}, \qquad 0 \le \rho \le R_{\text{vis}}. \tag{26}$$

The denominator $1 - e^{-A}$ ensures that the conditional PDF integrates to one over $[0, R_{\text{vis}}]$. The complementary event, in which no visible co-channel satellite exists, is counted as an outage in (24).

The conditional success probability given $\rho_0 = \rho$ is $p_{\text{succ}}^{\text{nearest}}(\rho;\tau)$ as given in (21). Multiplying the conditional average over (26) by the visibility probability $1 - e^{-A}$ yields the overall success probability

$$P_{\text{succ}}^{\text{nearest}}(\tau) = \int_0^{R_{\text{vis}}} 2\pi\lambda_c\rho\, e^{-\pi\lambda_c\rho^2} p_{\text{succ}}^{\text{nearest}}(\rho;\tau)\, d\rho. \tag{27}$$

Taking the complement gives

$$P_{\text{out}}^{\text{nearest}}(\tau) = 1 - P_{\text{succ}}^{\text{nearest}}(\tau),$$

which leads to (23). □

Unfortunately, the integral expression in (23) does not admit a closed form, which limits its analytical tractability and hinders system-level interpretation. To address this, we introduce the *EIP* approximation to express the outage probability in a concise and in-

sightful form. Specifically, EIP approximates the outer average over the serving distance by evaluating the conditional success probability at a representative distance, while retaining the interference integrals and finite SR sums.

Lemma 4. *The outage probability of the nearest-association rule can be approximated in a compact single-point form using the EIP approximation as*

$$\widetilde{P}_{\text{out}}^{\text{nearest}}(\tau) = 1 - (1 - e^{-A})\, p_{\text{succ}}^{\text{nearest}}(\hat{\rho}; \tau), \tag{28}$$

where

$$\hat{\rho} = R_{\text{vis}} \sqrt{\frac{1 - (1 + A)e^{-A}}{A(1 - e^{-A})}}. \tag{29}$$

Proof. Using (26), the nearest-association success probability can be expressed as

$$P_{\text{succ}}^{\text{nearest}}(\tau) = (1 - e^{-A}) \int_0^{R_{\text{vis}}} f_{\rho_0|\text{vis}}(\rho)\, p_{\text{succ}}^{\text{nearest}}(\rho; \tau)\, d\rho. \tag{30}$$

We approximate the conditional expectation above by a single evaluation at a representative point $\hat{\rho}$, defined as the root-mean-square of the truncated nearest-distance distribution:

$$\hat{\rho} = \sqrt{\mathbb{E}[\rho_0^2 \mid \rho_0 \le R_{\text{vis}}]} = R_{\text{vis}} \sqrt{\frac{1 - (1 + A)e^{-A}}{A(1 - e^{-A})}}. \tag{31}$$

Under the adopted geometry, $r^2(\rho) = H^2 + \rho^2$, so the root-mean-square (RMS) definition gives $r^2(\hat{\rho}) = \mathbb{E}[r^2(\rho_0) \mid \rho_0 \le R_{\text{vis}}]$. Thus, $\hat{\rho}$ is a representative projected distance that preserves the mean squared serving-link slant distance, conditioned on the existence of at least one visible co-channel satellite.

Accordingly,

$$P_{\text{succ}}^{\text{nearest}}(\tau) \approx (1 - e^{-A})\, p_{\text{succ}}^{\text{nearest}}(\hat{\rho}; \tau). \tag{32}$$

Taking the complement yields (28). □

For SINR-based evaluation with a fixed thermal noise power σ^2, the product of the interference Laplace transforms inside the derivative in (21) is multiplied by $e^{-z\sigma^2}$. The EIP expression (28) then applies with the resulting conditional success probability and the same representative distance $\hat{\rho}$.

Remark 2. *The EIP approximation (28) illustrates the impact of key parameters on outage behavior. Because the representative distance $\hat{\rho}$ in (29) depends on both the satellite density λ_c and the visibility radius R_{vis}, a larger satellite density generally reduces $\hat{\rho}$ and improves the serving-link geometry. Changes in altitude also affect $\hat{\rho}$ through R_{vis}, while simultaneously changing the probability of having a visible serving candidate. However, with the remaining system parameters fixed, increasing satellite density also increases aggregate interference. As the density grows, $\hat{\rho}$ approaches zero, but the serving-link slant distance approaches its positive lower limit H. Thus, further improvement in the serving-link geometry becomes limited, while interference continues to grow. Since the reuse factor F controls both the co-channel and leakage-interference densities, the EIP expression can also be used to examine reuse-factor sensitivity numerically. In addition, a smaller leakage-interference attenuation factor β or a lower decoding threshold τ further improves reliability, capturing the trade-off between outage performance and spectral efficiency.*

4. Numerical and Simulation Results

We evaluate the outage performance through simulations of the PPP-based LEO NTN model within a finite visibility disk and compare the results with the analytical expressions in Section 3. For the SINR evaluation, the fixed noise power corresponds to a mean overhead-link signal-to-noise ratio (SNR) of 10 dB. Unless otherwise stated, the simulation parameters and settings are summarized in Table 1.

Table 1. Common simulation parameters.

Parameter	Value	Parameter	Value
Altitude H [km]	600	$\theta_{\min}$ [°]	45
Beam activity p	0.30	Reuse factor F	4
Transmit power P_t	1	Path-loss α	2
Serving gain G_0	1.0	Co-channel G_I	0.04
Leakage factor β	0.01	Threshold τ_{dB}	2
SR parameter b	0.126	SR parameter Ω	0.835
SR parameter m	10	Mean overhead SNR [dB]	10 (SINR only)
Density λ_{sat} [km^{-2}]	25×10^{-6}		

Figure 2 shows the outage probability as a function of the satellite density λ_{sat} for the best- and nearest-association schemes under normalized SR fading with two decoding thresholds. As expected, the outage probability decreases as λ_{sat} increases over the considered density range because a denser constellation enhances the likelihood of having a nearby or high-SIR serving satellite. However, the improvement becomes more gradual as aggregate interference also increases with the active satellite density. Compared with best association, nearest association exhibits a higher outage probability but selects the serving satellite using only distance information, avoiding instantaneous SIR evaluation. This provides a practical trade-off between reliability and selection complexity. The analytical approximations in Lemmas 2 and 4 capture the overall outage trends of these two schemes. In particular, for nearest association, the EIP approximation closely matches both the simulation results and the numerical integral results from (23). This agreement supports replacing the serving-distance average with a single-point evaluation while maintaining good accuracy over the considered range.

Figure 3 depicts the outage probability of the nearest-association scheme as a function of the minimum elevation angle $\theta_{\min}$ for satellite altitudes $H = 400$, 600, and 800 km. The outage probability increases with $\theta_{\min}$ because a larger minimum elevation angle reduces the visibility radius $R_{\mathrm{vis}} = H/\tan\theta_{\min}$, leaving fewer active co-channel satellites available for serving-link selection. At a fixed $\theta_{\min}$, higher satellite altitudes yield lower outage probabilities. The expanded visibility region reduces the probability of having no active co-channel satellite. Although longer propagation distances increase path loss for both the desired and interfering signals, the improvement in serving-candidate availability dominates the outage behavior over the considered range.

Figure 4 illustrates the outage probability of the nearest-association scheme as a function of the reuse factor F for different SR fading parameter sets (b, Ω, m). The outage exhibits a non-monotonic dependence on F. As F increases from a small value, the outage probability initially decreases because the density of strong co-channel interferers is reduced. For larger F, however, the outage probability increases because the co-channel serving-candidate set becomes sparse, while the leakage-interference population grows. For a given reuse factor, lower outage probabilities are observed among the considered SR parameter sets when the line-of-sight component is more dominant and less variable. These characteristics reduce the severity of fading and improve link reliability.

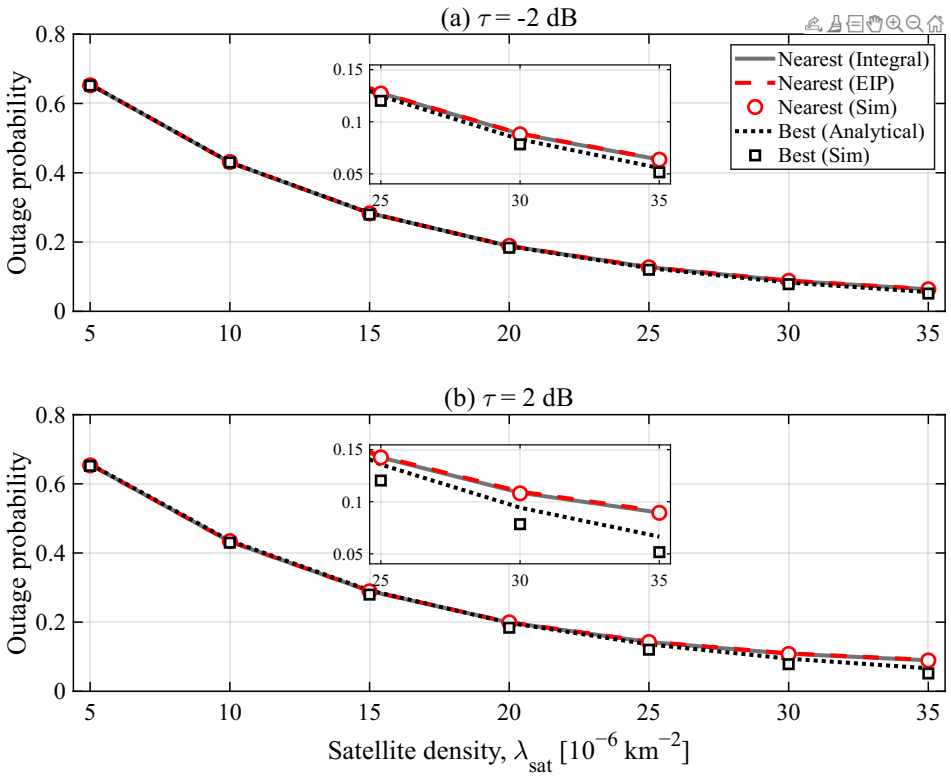


Figure 2. Outage probability versus satellite density λ_{sat} for the best- and nearest-association schemes under normalized SR fading, comparing simulations and analytical results under two decoding thresholds $\tau = -2$ dB and $\tau = 2$ dB. For nearest association, both the numerical integral results and the EIP approximation are shown.

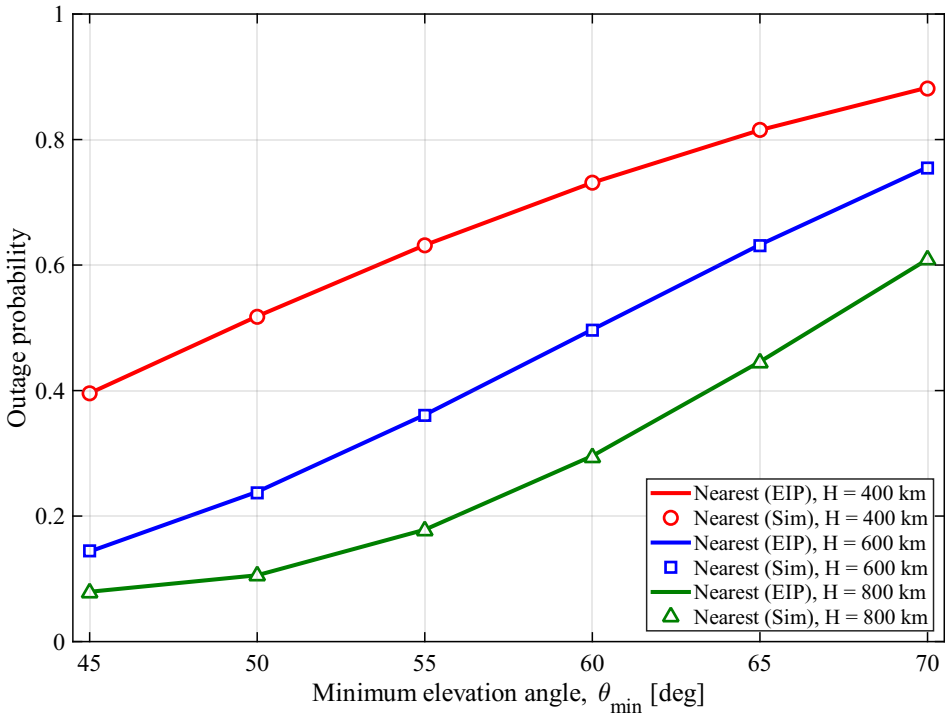


Figure 3. Outage probability of the nearest-association scheme versus the minimum elevation angle θ_{min} for satellite altitudes $H = 400$, 600, and 800 km, with $\lambda_{\text{sat}} = 25 \times 10^{-6}$ sat/km^2, $p = 0.30$, and $\tau = 2$ dB.

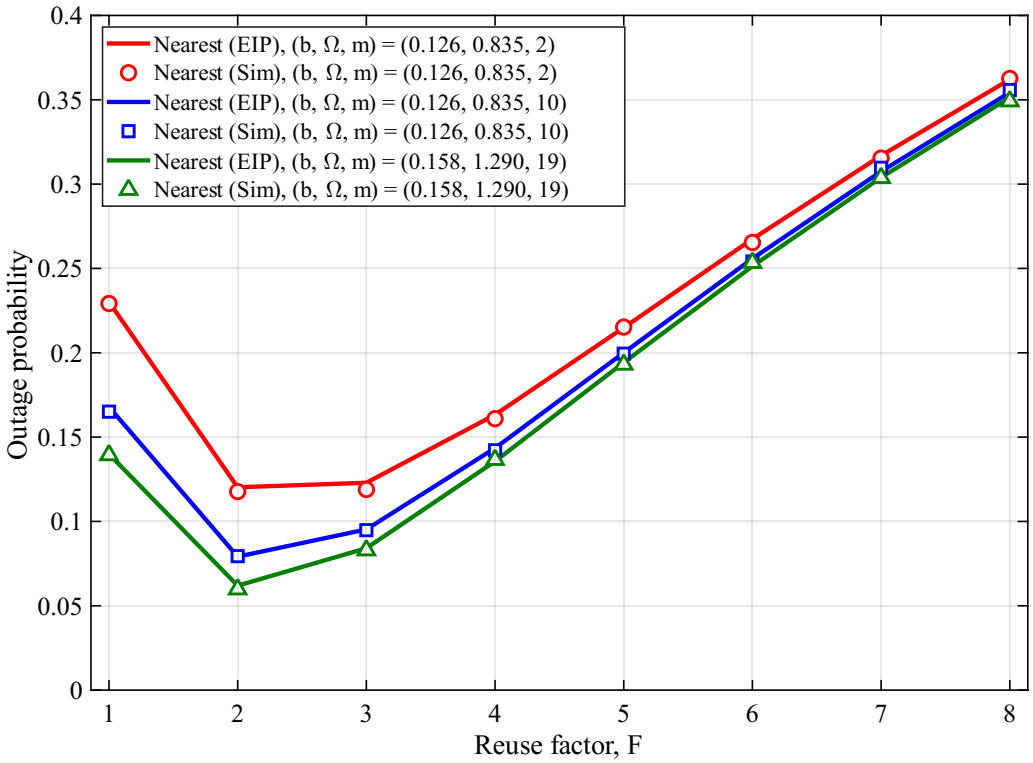


Figure 4. Outage probability of the nearest-association scheme versus the reuse factor F for different SR fading parameter sets (b, Ω, m), comparing simulations and the EIP approximation. The satellite density is $\lambda_{\text{sat}} = 25 \times 10^{-6}$ sat/km^2, and the decoding threshold is $\tau = 2$ dB.

Figure 5 shows the outage probability of the nearest-association scheme as a function of the full half-power beamwidth (HPBW) for two leakage factors β. This experiment employs a normalized directional antenna pattern [15], with fixed peak equivalent isotropically radiated power (EIRP) and perfect alignment of the serving beam toward the user. Each interfering beam points toward an independently selected ground location, uniformly distributed within a disk of radius R_{vis} centered at its satellite's nadir. For the EIP evaluation, the fading Laplace term is averaged over these beam directions at each interferer location before computing the interference integrals.

The outage probability increases with HPBW for both values of β. Broader interfering beams are more likely to illuminate the user with substantial antenna gain, increasing aggregate interference while the serving-link gain remains fixed. The outage probability is also higher for $\beta = 0.1$ than for $\beta = 0.01$, and the gap widens as HPBW increases. The larger β corresponds to weaker leakage attenuation, making reliability more sensitive to the increased interference from broader beams. The EIP approximation captures these performance trends, although it slightly overestimates the outage probability at wider beamwidths.

Figure 6 shows the outage probability of nearest association versus satellite density λ_{sat} under SIR and SINR criteria. The outage probability initially decreases with satellite density because more active co-channel satellites become available for serving-link selection. At sufficiently high densities, however, the outage probability increases and approaches one. This is because the serving-link distance cannot decrease below the altitude H, which limits further path-loss improvement, while aggregate interference continues to grow. The SINR results follow the same overall trend as the SIR results, although thermal noise increases the outage probability.

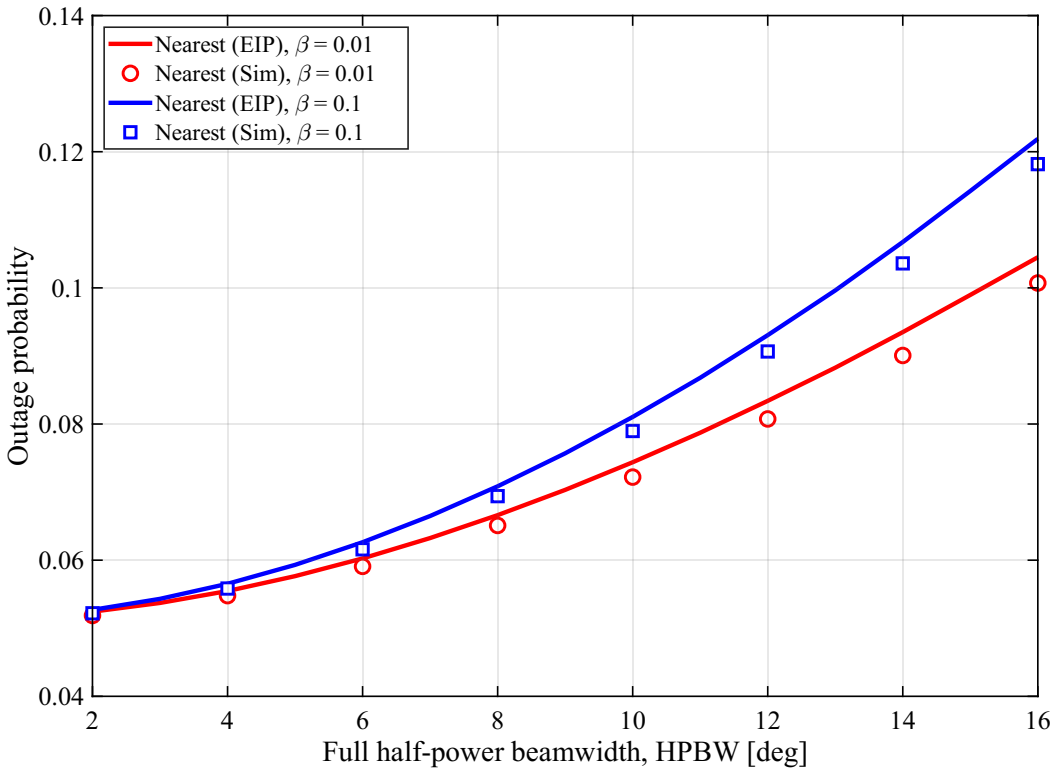


Figure 5. Outage probability of the nearest-association scheme versus the full half-power beamwidth (HPBW) for $\beta = 0.01$ and 0.1, comparing simulations and the EIP approximation. The satellite density is $\lambda_{\text{sat}} = 35 \times 10^{-6}$ sat/km^2, with $F = 4$ and $\tau = 2$ dB.

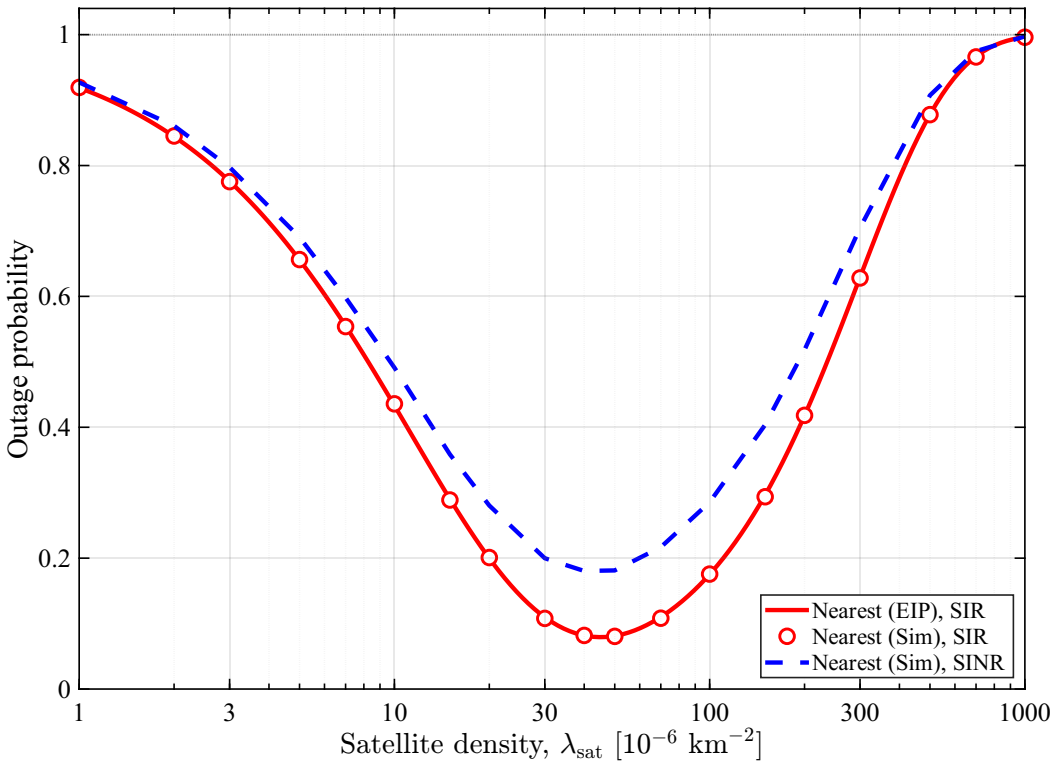


Figure 6. Outage probability of the nearest-association scheme versus satellite density λ_{sat} under SIR and SINR criteria, comparing simulations and the EIP approximation, with $F = 4$ and $\tau = 2$ dB. For the SINR case, the fixed noise power corresponds to a mean overhead-link SNR of 10 dB.

5. Conclusions

This paper presented a tractable analytical framework for evaluating the outage performance of large-scale LEO satellite constellations. Using a ground-projected PPP model, we compared best and nearest association under finite visibility, beam-hopping activity, and normalized SR fading. An EIP approximation was developed to enable accurate and computationally efficient performance evaluation without numerical averaging over the nearest-satellite distance distribution.

The results show that nearest association incurs higher outage than best association but avoids instantaneous SIR evaluation by relying only on distance information, offering a practical trade-off between reliability and selection complexity. For nearest association, increasing satellite density initially improves reliability, but excessive densification eventually increases outage as aggregate interference grows while further serving-distance improvement becomes limited. Future work will consider extensions to spherical constellation geometry and temporally correlated beam-hopping activity.

Author Contributions: Conceptualization, J.B. and T.K.; methodology, J.B.; software, J.B.; validation, J.B. and T.K.; formal analysis, J.B.; investigation, J.B. and T.K.; visualization, J.B.; writing—original draft preparation, J.B.; writing—review and editing, T.K.; funding acquisition, T.K. All authors have read and agreed to the published version of the manuscript.

Funding: This work was supported by the Institute of Information and Communications Technology Planning and Evaluation (IITP) through Korean Government (MSIT) under Grant RS-2024-00397789 (Development and Standardization of 6G Radio Transmission Standard Technology).

Data Availability Statement: The original contributions presented in this study are included in the article. Further inquiries can be directed to the corresponding author.

Conflicts of Interest: The authors declare no conflict of interest.

Appendix A

Table A1. Notations used throughout the paper.

Notation	Definition
λ_{sat}	Spatial density of ground-projected satellites
H	Satellite altitude
ρ	Ground-projected distance between the user and a satellite
$r(\rho)$	User–satellite slant distance, $r(\rho) = \sqrt{H^2 + \rho^2}$
$\theta(\rho)$	Elevation angle of a satellite at projected distance ρ
$\theta_{\min}$	Minimum elevation angle required for satellite visibility
R_{vis}	Radius of the ground-projected satellite visibility region
$\mathcal{D}_{\text{vis}}$	Ground-projected satellite visibility region
λ_{act}	Spatial density of active satellites, $\lambda_{\text{act}} = \lambda_{\text{sat}} p$
Φ_c, λ_c	PPP and spatial density of active co-channel satellites
Φ_ℓ, λ_ℓ	PPP and spatial density of leakage-interference satellites
P_t	Satellite transmit power
G_0	Effective antenna gain of the serving link
G_I	Effective antenna gain of a co-channel interfering link
β	Leakage-interference attenuation factor
h	Normalized shadowed-Rician (SR) fading power gain, $\mathbb{E}[h] = 1$
α	Path-loss exponent
τ	SIR decoding threshold
$\mathcal{L}_{I_c}, \mathcal{L}_{I_\ell}$	Laplace transforms of the co-channel and leakage interference, respectively
$s^\star, \rho^\star$	Serving satellite and its projected distance under best association
ρ_0	Projected distance to the nearest active co-channel satellite

References

1. Darwish, T.; Kurt, G.K.; Yanikomeroglu, H.; Bellemare, M.; Lamontagne, G. LEO Satellites in 5G and Beyond Networks: A Review from a Standardization Perspective. *IEEE Access* **2022**, *10*, 35040–35060. [CrossRef]
2. Azari, M.M.; Solanki, S.; Chatzinotas, S.; Kodheli, O.; Sallouha, H.; Colpaert, A.; Mendoza Montoya, J.F.; Pollin, S.; Haqiqatnejad, A.; Mostaani, A.; et al. Evolution of Non-Terrestrial Networks From 5G to 6G: A Survey. *IEEE Commun. Surv. Tutor.* **2022**, *24*, 2633–2672. [CrossRef]
3. Leyva-Mayorga, I.; Soret, B.; Röper, M.; Wübben, D.; Matthiesen, B.; Dekorsy, A.; Popovski, P. LEO Small-Satellite Constellations for 5G and Beyond-5G Communications. *IEEE Access* **2020**, *8*, 184955–184964. [CrossRef]
4. Ying, K.; Gao, Z.; Chen, S.; Zhou, M.; Zheng, D.; Chatzinotas, S.; Ottersten, B.; Poor, H.V. Quasi-Synchronous Random Access for Massive MIMO-Based LEO Satellite Constellations. *IEEE J. Sel. Areas Commun.* **2023**, *41*, 1702–1722. [CrossRef]
5. Liu, S.; Gao, Z.; Wu, Y.; Ng, D.W.K.; Gao, X.; Wong, K.K.; Chatzinotas, S.; Ottersten, B. LEO Satellite Constellations for 5G and Beyond: How Will They Reshape Vertical Domains? *IEEE Commun. Mag.* **2021**, *59*, 30–36. [CrossRef]
6. Heydarishahreza, N.; Han, T.; Ansari, N. Spectrum Sharing and Interference Management for 6G LEO Satellite–Terrestrial Network Integration. *IEEE Commun. Surv. Tutor.* **2024**, *27*, 2794–2825. [CrossRef]
7. Kim, D.; Jung, H.; Lee, I.H.; Niyato, D. Multi-Beam Management and Resource Allocation for LEO Satellite-Assisted IoT Networks. *IEEE Internet Things J.* **2025**, *12*, 19443–19458. [CrossRef]
8. Tong, J.; Wang, C.; Zhao, X.; Cui, G.; Wang, W. Cooperative Beam Association and Power Allocation in UD-LEO Satellite Communication Networks: A Spectrum Sharing Manner. *Electronics* **2022**, *11*, 299. [CrossRef]
9. Guo, S.; Han, K.; Gong, W.; Li, L.; Tian, F.; Jiang, X. An Efficient Multi-Dimensional Resource Allocation Mechanism for Beam-Hopping in LEO Satellite Network. *Sensors* **2022**, *22*, 9304. [CrossRef] [PubMed]
10. Massad, M.A.; Alma'aitah, A.Y.; Hassanein, H.S. Real-Time Handover in LEO Satellite Networks via Markov Chain-Guided Simulated Annealing. *Network* **2025**, *5*, 49. [CrossRef]
11. Wang, R.; Kishk, M.A.; Alouini, M.S. Stochastic Geometry-Based Low Latency Routing in Massive LEO Satellite Networks. *IEEE Trans. Aerosp. Electron. Syst.* **2022**, *58*, 3881–3894. [CrossRef]
12. Hong, T.; Yu, X.; Liu, Z.; Ding, X.; Zhang, G. Narrowband Internet of Things via Low Earth Orbit Satellite Networks: An Efficient Coverage Enhancement Mechanism Based on Stochastic Geometry Approach. *Sensors* **2024**, *24*, 2004. [CrossRef] [PubMed]
13. Giordani, M.; Zorzi, M. Non-Terrestrial Networks in the 6G Era: Challenges and Opportunities. *IEEE Netw.* **2021**, *35*, 244–251. [CrossRef]
14. Okati, N.; Riihonen, T.; Korpi, D.; Angervuori, I.; Wichman, R. Downlink Coverage and Rate Analysis of Low Earth Orbit Satellite Constellations Using Stochastic Geometry. *IEEE Trans. Commun.* **2020**, *68*, 5120–5134. [CrossRef]
15. Kim, E.; Roberts, I.P.; Andrews, J.G. Downlink Analysis and Evaluation of Multi-Beam LEO Satellite Communication in Shadowed Rician Channels. *arXiv* **2022**, arXiv:2207.06663.
16. Baccelli, F.; Blaszczyszyn, B. *Stochastic Geometry and Wireless Networks, Volume I: Theory*; NOW Publishers: Norwell, MA, USA, 2009.
17. Haenggi, M. *Stochastic Geometry for Wireless Networks*; Cambridge University Press: Cambridge, UK, 2012.
18. 3GPP. *Study on New Radio (NR) to Support Non-Terrestrial Networks*, Version 15.4.0; Technical Report (TR) 38.811; 3rd Generation Partnership Project (3GPP): Sophia Antipolis Cedex, France, 2020.
19. 3GPP. *Solutions for NR to Support Non-Terrestrial Networks (NTN)*, Version 16.2.0; Technical Report (TR) 38.821; 3rd Generation Partnership Project (3GPP): Sophia Antipolis Cedex, France, 2023.
20. Abdi, A.; Lau, W.C.; Alouini, M.-S.; Kaveh, M. A New Simple Model for Land Mobile Satellite Channels: First- and Second-Order Statistics. *IEEE Trans. Wirel. Commun.* **2003**, *2*, 519–528. [CrossRef]

Disclaimer/Publisher's Note: The statements, opinions and data contained in all publications are solely those of the individual author(s) and contributor(s) and not of MDPI and/or the editor(s). MDPI and/or the editor(s) disclaim responsibility for any injury to people or property resulting from any ideas, methods, instructions or products referred to in the content.